Effects of background gas pressure on the dynamics of a nonneutral electron plasma confined in a Malmberg–Penning trap

Edward H. Chao, Ronald C. Davidson,[a] Stephen F. Paul, and Kyle A. Morrison
Plasma Physics Laboratory, Princeton University, Princeton, New Jersey 08543

(Received 4 October 1999; accepted 7 December 1999)

The effects of electron–neutral collisions on plasma expansion properties and the evolution of the $m=1$ diocotron mode are investigated in the Electron Diffusion Gauge (EDG) experiment, a Malmberg–Penning trap with plasma length $L_p \simeq 15$ cm, plasma radius $R_p \simeq 1.3$ cm, and characteristic electron density $5\times10^6\,\mathrm{cm}^{-3} < n < 3\times10^7\,\mathrm{cm}^{-3}$. Essential features of the $m=1$ diocotron mode dynamics in the absence of electron–neutral collisions are verified to behave as expected. The mode frequency, the growth rate of the resistive-wall instability, and the frequency shift at nonlinearly large amplitudes are all in good agreement with theoretical predictions. When helium gas is injected into the trap, the evolution of the mode amplitude is found to be very sensitive to the background gas pressure down to pressures of 5×10^{-10} Torr, the lowest base pressure achieved in the EDG device. The characteristic time scale τ for nonlinear damping of the $m=1$ diocotron mode is observed to scale as $P^{-1/2}$ over two orders-of-magnitude variation in the background gas pressure P. The evolution of the plasma density profile has also been monitored in order to examine the shape of the evolving density profile $n(r,t)$ and to measure the expansion rate. The density profile is observed to expand radially while maintaining a thermal equilibrium profile shape, as predicted theoretically. While the expansion rate is sensitive to background gas pressure at pressures exceeding 10^{-8} Torr, at lower pressures the cross-field transport appears to be dominated by other processes, e.g., asymmetry-induced transport. Finally, the expansion rate is observed to scale approximately as $B^{-3/2}$ for confining fields ranging from 100 to 600 G. © *2000 American Institute of Physics.* [S1070-664X(00)03403-0]

I. INTRODUCTION

Understanding the dynamics of a nonneutral electron plasma[1,2] interacting with background neutral gas[3–8] may result in a reliable method of determining high vacuum pressures, or if the vacuum pressure is known, of determining the electron–neutral collision cross section. A detailed understanding of the effects of background neutrals on nonneutral plasma confined in a Malmberg–Penning trap (Fig. 1) is also important in other experiments that investigate the fundamental properties of nonneutral plasmas. Nonneutral plasmas are used in research to develop atomic clocks,[9,10] studies of turbulence, nonlinear vortex dynamics, and instabilities in nearly inviscid two-dimensional fluids,[11–13] studies of particle transport across magnetic field lines in quiescent plasmas,[14] studies of the properties of nonneutral plasmas in thermal equilibrium,[15,16] and in experiments to study the formation and confinement of positron plasmas.[17–19] Many of these experiments are performed at vacuum pressures in the range[9,13–19] where background neutrals are observed[3–6] to affect the plasma dynamical behavior and confinement properties.

This paper summarizes recent experimental studies[3,4] of the effects of background gas pressure on the expansion of the electron density profile and the nonlinear dynamics of the $m=1$ diocotron mode in the Electron Diffusion Gauge (EDG) experiment, extending the earlier experimental results[5,6] obtained on the EDG device. Following a description of the experimental setup (Sec. II), in Sec. III the scaling of the plasma expansion rate with background gas pressure P and magnetic-field strength B is investigated, based on direct measurements of the expanding density profile $n(r,t)$. In Sec. IV, the detailed dynamics of the $m=1$ diocotron mode is investigated over a wide range of background gas pressure P. It is found that the evolution of the $m=1$ diocotron mode exhibits a strong sensitivity to the background gas pressure, and that the time scale τ for damping of the diocotron mode scales as $P^{-1/2}$.

II. ELECTRON DIFFUSION GAUGE (EDG) EXPERIMENTAL SETUP

As illustrated in Fig. 2, the pure electron plasma in the Electron Diffusion Gauge (EDG) device[3–6] is confined in a cylindrical Malmberg–Penning trap, with a uniform axial magnetic field $B\hat{\mathbf{e}}_z$ providing radial confinement, and applied voltages on end cylinders providing axial confinement. In Fig. 2, the colinear, cylindrical electrodes have an inner radius of $R_w = 2.54$ cm and the applied end potentials are typically 145 V. The magnetic field is generated by a solenoid with a current profile tailored such that the axial field amplitude variation in the trap region is less than 0.2%. The current is varied to generate magnetic field strengths in the range $100\ \mathrm{G} < B < 600\ \mathrm{G}$. The entire trap is contained in a vacuum chamber with a base pressure of 5×10^{-10} Torr. A turbomo-

[a]Electronic mail: rdavidson@pppl.gov

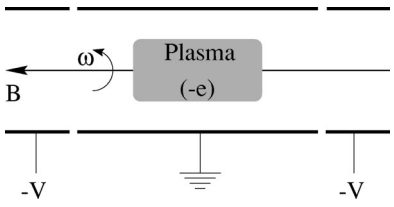

FIG. 1. Essential features of a Malmberg–Penning trap confining a pure electron plasma. Transverse confinement of the electrons is provided by the axial magnetic field $B\hat{\mathbf{e}}_z$, whereas axial confinement is provided by negative voltages applied to the end cylinders.

lecular pump and a cryogenic pump are located on opposite ends of the trap. Pressures are measured with two ultrahigh vacuum (UHV) Bayard–Alpert ionization gauges, also located on opposite ends of the trap. These gauges have not been calibrated, and therefore, errors in their absolute sensitivities[20,21] may be as large as 50%. Nevertheless, the *relative* changes in the measured pressure are expected to be reliable.[16] Purified helium gas is then injected to achieve a constant and controllable background neutral pressure with known composition, although a residual gas analyzer has not yet been installed. A relative sensitivity of five is used when determining true helium pressures from the ionization gauges.

The source of plasma electrons is thermionic emission from a thoriated tungsten filament wound in a spiral shape with an outer diameter of 2.54 cm ($R_f = 1.27$ cm). The filament is immersed in the uniform magnetic field and resistively heated by passing a direct current through it. Emitted electrons stream along the magnetic field into the trapping region, producing a column of electron plasma. The spiral geometry and the voltage drop due to the heating current provide an approximate match between the cathode electrostatic potential and the potential arising from the space-charge electric field of a uniform density electron column.[22,23] Thus, the plasma density and the number of electrons per unit axial length are controllable through the filament parameters.

The trap is operated with repeated cycles consisting of inject, hold, and dump phases.[3–6] During the inject phase, all of the wall cylinders are grounded except for the dump electrode (labeled electrode No. 5 in Fig. 2) which is biased negatively, producing a column of electrons between the filament and the dump electrode. A portion of the plasma column is then trapped by biasing electrode No. 1 negatively. After a variable ''hold'' time, the dump gate potential is pulsed to ground, allowing the electrons to stream out axially along the magnetic field lines to the collector. The collector assembly consists of a plate with a small collimating hole ($R_h = 0.159$ cm), and can be moved radially. Behind the hole in the collimator plate is a Faraday cup. The majority of electrons are collected on the collimator plate producing a voltage across the distributed capacitance of the plate and detector electronics. A much smaller number of electrons falls on the Faraday cup, producing a separate voltage reading.

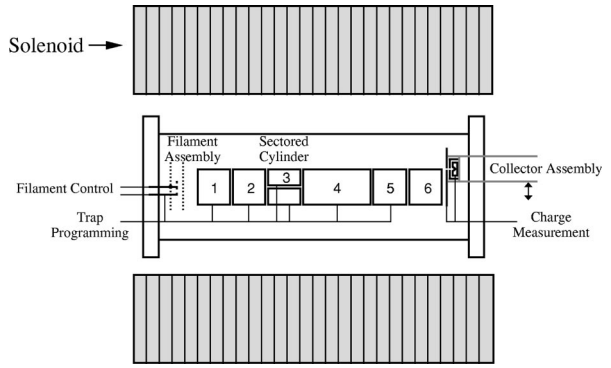

FIG. 2. Schematic of the Malmberg–Penning trap used in the Electron Diffusion Gauge (EDG) experiment showing the six electrically-isolated, colinear cylinders as well as the electron source and diagnostics.

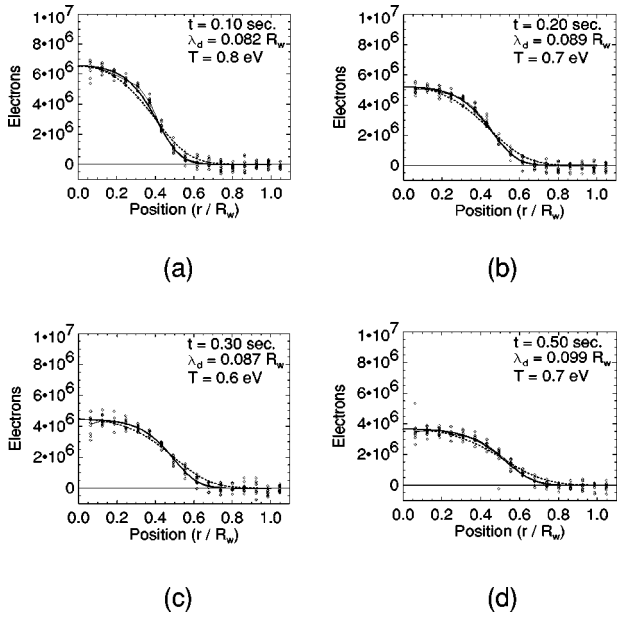

FIG. 3. Time evolution of the measured density profile is shown in (a)–(d). Each density profile shows the number of electrons measured at each radial location, $Q(r)/(-e) = A_h \int dz\, n(r,z)$. Also plotted is the best-fit solution to Eqs. (3) and (4) for each profile. The line density N_L for each profile is approximately 3.2×10^7 cm^{-1}, and the background neutral pressure is 2×10^{-8} Torr. The experimental uncertainty is approximately 10% in the Debye length λ_d and 20% in the temperature T.

Scanning the collimator radially while repeating the cycle of inject, hold, and dumping allows a determination of the z-integrated charge density profile,

$$Q(r) = -eA_h \int dz n(r,z), \tag{1}$$

where $-e$ is the electron charge, A_h is the area of the collimator hole, $n(r,z)$ is the electron density profile, and r is the radial distance from the cylinder axis. The density measurements depend on the excellent shot-to-shot reproducibility of the plasmas. Fluctuations in the total charge trapped (measured on the collimating plate) from shot to shot are typically less than 0.5%. The fluctuations in the charge measured through the collimating hole in Fig. 2 are dominated by external noise. Typical experimental results for the expanding radial density profiles in the EDG device are presented in Fig. 3, and also in Fig. 2 of Ref. 5.

From the data for $Q(r)$, the density profile $n(r,z)$ may be reconstructed by assuming that the electrons are in thermal equilibrium along magnetic field lines such that

$$n(r,z)=\frac{1}{-eA_h\int dz\,\exp[e\phi(r,z)k_BT]}\,Q(r)\exp[e\phi(r,z)/k_BT], \tag{2}$$

where k_B is Boltzmann's constant, and T is the electron temperature. Note that the normalization in Eq. (2) assures that Eq. (1) is automatically satisfied. Solving Eq. (2) together with Poisson's equation

$$\left\{\frac{1}{r}\frac{\partial}{\partial r}r\frac{\partial}{\partial r}+\frac{\partial^2}{\partial z^2}\right\}\phi(r,z)=-4\pi en(r,z), \tag{3}$$

and using the known potentials on the trap walls as boundary conditions allow the determination of the density and potential profiles numerically.[24] The trapped electron plasma has initial density of $5\times10^6\,\mathrm{cm}^{-3}<n<3\times10^7\,\mathrm{cm}^{-3}$, temperature of about 1 eV, radius $R_p\simeq1.3$ cm, and length $L_p\simeq15$ cm. An electron temperature of about 1 eV is typical of similar Malmberg–Penning trap experiments.[25] For these parameters, the Debye length, $\lambda_D=(k_BT/4\pi ne^2)^{1/2}$, is much smaller than the diameter of the plasma ($2R_p\simeq12\lambda_D$), and $\omega_{pe}^2/\omega_{ce}^2<0.01$. Here, $\omega_{pe}=(4\pi ne^2/m_e)^{1/2}$ is the electron plasma frequency, and $\omega_{ce}=eB/m_ec$ is the electron cyclotron frequency in the confining magnetic field $B\hat{\mathbf{e}}_\mathbf{z}$. Because the plasma is nonneutral, there is a strong self-electric field in the radial direction which, in conjunction with the uniform axial magnetic field $B\hat{\mathbf{e}}_\mathbf{z}$, causes the plasma electrons to undergo an $\mathbf{E}\times\mathbf{B}$ rotation. In thermal equilibrium, the angular rotation velocity is independent of radius r, and the plasma rotates like a rigid rotor with characteristic rotation frequency in the range $10^5\,\mathrm{Hz}<\omega_0/2\pi<10^6$ Hz.

III. PLASMA EXPANSION MEASUREMENTS

In this section, we summarize recent experimental results[3,4] on the expansion of the electron density profile in the EDG device, extending our earlier studies[5] to determine the scaling of the plasma expansion rate with background gas pressure P and magnetic field strength B.

A. Change in mean-square radius and electrostatic field energy

By way of background, in a recent calculation[7,8] assuming elastic collisions between the electrons and background neutral atoms with constant collision frequency ν_{en}, a macroscopic fluid model was used to describe the collisional relaxation of a strongly magnetized ($\omega_{pe}^2\ll\omega_{ce}^2$) pure electron plasma with isothermal electrons (T=const.), assuming a long, axisymmetric plasma column with $\partial/\partial z=0=\partial/\partial\theta$. It was shown[7] that electron–neutral collisions cause the electron density profile $n(r,z)$ to relax to a dynamically expanding (thermal equilibrium) profile of the form

$$n(r,t)=\hat{n}(t)\exp\left\{\frac{e\phi(r,t)-e\hat{\phi}(t)}{k_BT}-\frac{r^2}{\langle r^2\rangle(t)}\left(1+\frac{N_Le^2}{2k_BT}\right)\right\}. \tag{4}$$

In Eq. (4), $\phi(r,t)$ is the electrostatic potential determined self-consistently from Poisson's equation, $\hat{\phi}(t)\equiv\phi(r=0,t)$ and $\hat{n}(t)\equiv n(r\simeq0,t)$ are the on-axis potential and density, respectively, k_B is Boltzmann's constant, $-e$ is the electron charge, $N_L=2\pi\int_0^{R_w}drrn(r,t)=$const. is the line density, and $\langle r^2\rangle(t)=N_L^{-1}2\pi\int_0^{R_w}drrr^2n(r,t)$ is the mean-square radius of the plasma column. In addition, the mean-square radius $\langle r^2\rangle(t)$ is predicted to increase due to electron–neutral collisions according to[7]

$$\frac{d}{dt}\langle r^2\rangle=\frac{2N_Le^2}{m_e\omega_{ce}\omega_{ce}}\nu_{en}\left(1+\frac{2k_BT}{N_Le^2}\right), \tag{5}$$

where $\omega_{ce}=eB/m_ec$ is the electron cyclotron frequency.

The remarkably simple form of the classical predictions in Eqs. (4) and (5) are amenable to direct experimental measurement. In recent experiments[5] on the EDG device, carried out in a regime where the initial plasma density profile is not too irregular (e.g., hollow), it was found[26] that the experimental density profiles, measured in repeated hold-and-dump cycles, fit remarkably well to the expanding thermal equilibrium shape in Eq. (4), using one adjustable parameter (the electron temperature) at fixed line density N_L (see Fig. 3). There are two notable anomalies in the data, however. First, the measured expansion rate,[5] although increasing with background gas pressure, is anomalously fast in comparison with Eq. (5), likely due to enhanced radial diffusion caused by field asymmetries.[27] Second, the best-fit values of the electron temperature (not measured directly) consistent with Eq. (4) and the measured profile shape for $n(r,t)$ remain relatively constant[5] (between 0.7 and 0.9 eV). This is true even though the relatively large decrease[5] in electrostatic field energy (1 to 2 eV per particle) would be expected to result in a sizeable increase in electron temperature, if the electron–neutral collisions are elastic and the total plasma energy is conserved.[3–5]

Using the detailed measurements[3] of the electron density profiles $n(r,t)$ in the EDG device, the mean-square radius, $\langle r^2\rangle(t)$, and the electrostatic field energy per particle, $W_f(t)$, are calculated from

$$\langle r^2\rangle(t)=\frac{2\pi}{N_L}\int_0^{R_w}drrr^2n(r,t), \tag{6}$$

$$W_f(t)=-\frac{2\pi}{N_L}\int_0^{R_w}drr\frac{1}{2}e\phi(r,t)n(r,t). \tag{7}$$

Typical results are illustrated in Figs. 4 and 5, which show plots of $\langle r^2\rangle(t)$ and $W_f(t)$ versus time t at various background helium gas pressures. Although the experimental results in Fig. 4 are in qualitative agreement with Eq. (5) (the expansion is faster at higher background gas pressures), the absolute rate of expansion in Fig. 4 is much faster than that predicted by Eq. (5) (see also Fig. 6), likely due to radial transport induced by field asymmetries.[27] As the plasma expands, there is a corresponding sizeable decrease in electrostatic field energy $W_f(t)$, as evident from Fig. 5. The plots in Fig. 5 are for the same data sets as the plots of the evolution of the mean-square radius shown in Fig. 4, and the instantaneous radial density profiles shown in Fig. 3.

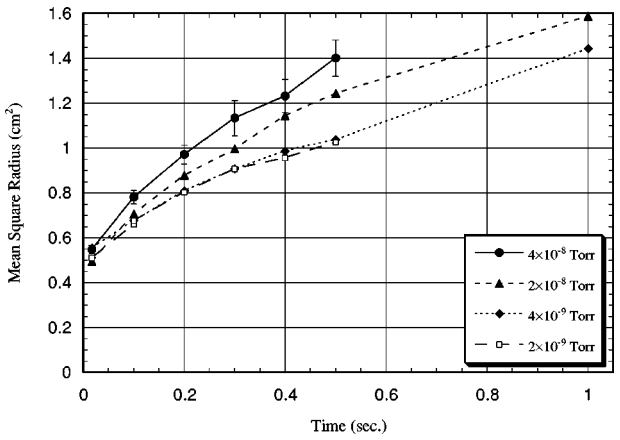

FIG. 4. The plasma mean-square radius increases with time, with the expansion rate depending on the background neutral gas pressure as shown. The expansion rates also depend on the magnetic field strength, which was 200 G for the data shown here.

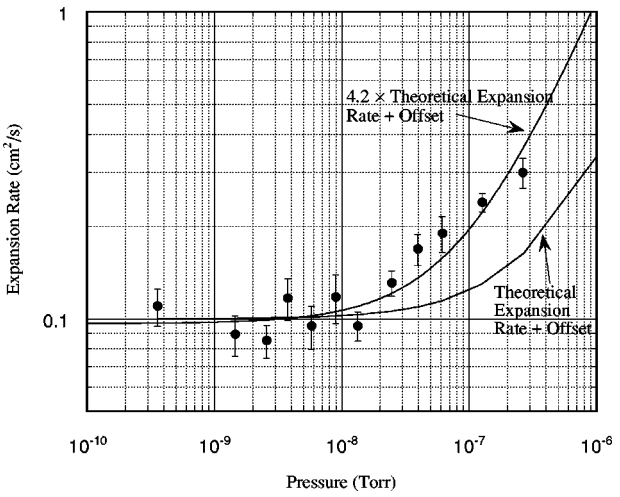

FIG. 6. The measured plasma expansion rates ($d\langle r^2\rangle/dt$) are plotted versus background neutral helium pressure. The expansion rates predicted by Eq. (5) have also been added, where a constant offset in the expansion rates has been added.

If the electron–neutral collisions are elastic and the total plasma energy is conserved, then the decrease in $W_f(t)$ in Fig. 5 would be compensated by a corresponding increase in the plasma kinetic energy (directed rotational energy and/or electron temperature T). For the plasma parameters in the EDG device, it is found[3] that the rotational kinetic energy per unit length is small in comparison with $(3/2)N_L k_B T$. From Fig. 5, setting $k_B \Delta T = -(\frac{2}{3})\Delta W_f$ would give electron temperature increases approaching 0.9 eV. As noted earlier, this is inconsistent with the ''best-fit'' temperatures[5] inferred from Eq. (1), and the experimentally measured density profiles $n(r,t)$. Indeed, the best-fit values of T show a slight decrease[5] in electron temperature as the plasma expands, which is also consistent with Eq. (5) and the (slight) downward concavity[8] of the plots of $\langle r^2\rangle(t)$ versus t in Fig. 4. A likely cause for energy loss from the plasma is through inelastic collisions with either the majority background helium atoms or other residual gas atoms present. The predicted loss of energy by electrons through collisions with the helium atoms is minimal, with a characteristic energy-loss time of $4(m_e/M)\nu_{en}$, where m_e is the electron mass, M is the mass of a helium atom, and ν_{en} is the electron-helium collision frequency. At a pressure of 1×10^{-8} Torr, the predicted collision frequency ν_{en} is approximately $10\,s^{-1}$, and the characteristic energy transfer time would be greater than 10^2 s. Collisions with other trace neutral gas atoms present in the system, including polyatomic molecules such as H_2, N_2, CO, CO_2, H_2O, etc., are much less frequent than collisions with helium atoms, but the energy exchange can be far greater.

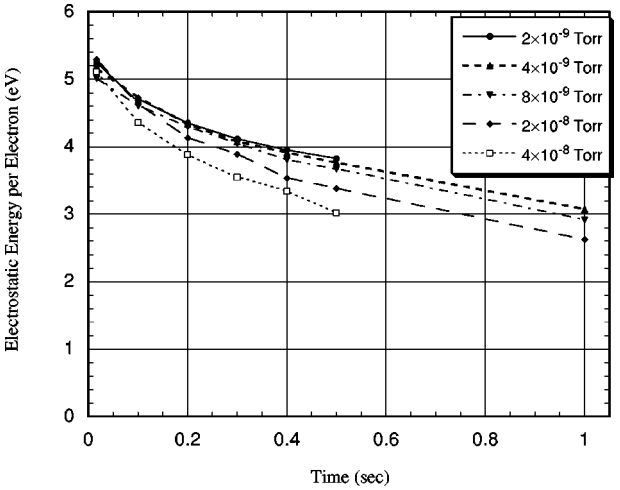

FIG. 5. The electrostatic field energy is calculated numerically using the measured radial density profile (Refs. 3–5) As the plasma expands, the electrostatic field energy decreases.

B. Expansion rate scaling with background gas pressure *P* and magnetic field *B*

While earlier experiments[27,28] have measured the evolution of the central density and the total charge trapped over a wide range of background gas pressure P and magnetic field strength B, these experiments did not give a detailed characterization of the evolution of the density profile $n(r,t)$ as has been done in the EDG device.[3–5] Using the experimentally measured[3] density profiles to calculate $\langle r^2\rangle(t)$ from Eq. (6), Figs. 6 and 7 show typical experimental results obtained in the EDG device in which the measured expansion rate, $(d/dt)\langle r^2\rangle$, is plotted versus background helium gas pressure P (Fig. 6) and magnetic field strength B (Fig. 7).

In Fig. 6, beginning with a base pressure of approximately 3×10^{-10} Torr, purified helium gas is injected into the EDG device to increase the pressure in controlled amounts. The measurements shown in Fig. 6 were performed at a constant plasma line density $N_L = 4.0\times10^7\,cm^{-1}$, magnetic field $B = 610$ G, and temperature $T = 1$ eV. If the cause of the plasma expansion were primarily due to electron–neutral collisions, the expansion rate would be expected to scale linearly with pressure, and the data shown in Fig. 6 would exhibit a decade increase in expansion rate per decade increase in pressure. This is clearly not the case. Instead, the expansion rate reaches a saturation level at pressures below

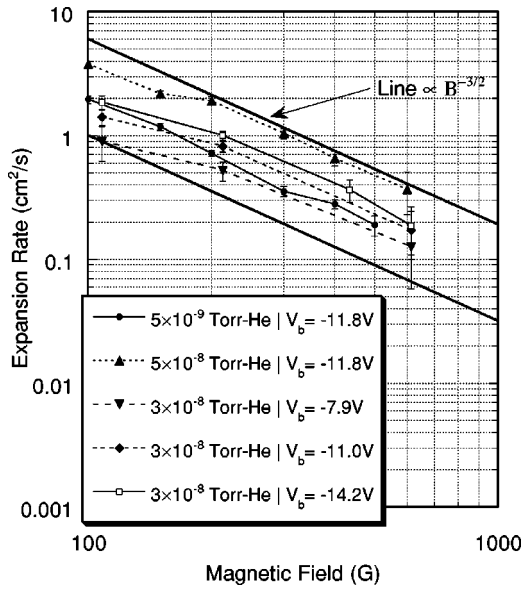

FIG. 7. The measured expansion rate of the mean-square radius ($d\langle r^2\rangle/dt$) is shown as a function of the magnetic field strength B. Five different experimental conditions are plotted corresponding to pressures ranging from 5×10^{-9} Torr to 5×10^{-8} Torr and line densities ranging from 2×10^{7} cm^{-1} to 4×10^{7} cm^{-1}.

10^{-8} Torr and does not continue to decrease at lower pressures. The cause of the saturation is likely due to asymmetry-induced radial transport,[27] which is independent of background gas pressure.

The solid curves shown in Fig. 6 correspond to the expansion rate predicted by Eq. (5), where a constant offset has been added to the prediction to account for transport caused by factors independent of background gas pressure (e.g., asymmetry-induced transport). The lower curve gives the predicted expansion rate with no adjustable parameters other than the constant offset. The upper curve is a best-fit line allowing an adjustable multiplying factor to the predicted expansion rate in Eq. (5). Allowing for a constant multiplying factor in Fig. 6 compensates for the uncertainty in the absolute background pressure due to the uncalibrated ionization gauges. At increasing pressures, electron–neutral collisions will become the dominant factor causing plasma expansion and the expansion rate is expected to increase linearly with background gas pressure. Future experiments on the EDG device will include investigation of plasma expansion at higher background gas pressure. However, in the present studies, the plasma expansion is measured only for pressures on the order of 10^{-7} Torr or less so that the plasma temperature can be assumed to be approximately uniform.[3,5]

The data in Fig. 6 are obtained at a constant magnetic field of 610 G. Varying the magnetic field will also change the expansion rates according to Eq. (5), with the expansion rate predicted to scale as B^{-2}. Again, this assumes that the expansion is caused by electron–neutral collisions. In Fig. 7, the expansion rate is plotted as a function of the magnetic field strength, for five different combinations of the background gas pressure and the plasma line density. The background gas pressure ranges from 5×10^{-9} Torr to 5×10^{-8} Torr, and the line density ranges from 2×10^{7} to 4×10^{7} cm^{-1}. The solid lines plotted in Fig. 7 are proportional to $B^{-3/2}$. For this range of experimental parameters, the scaling of the expansion rates is closer to $B^{-3/2}$, rather than the B^{-2} scaling predicted by Eq. (5).

This discrepancy in the scaling rate with magnetic field may be due to the same anomalous factors that contribute to the plasma expansion rate. One possible factor mentioned previously is asymmetries in the confining fields. This effect has been studied[29] by applying a potential to an asymmetric patch in the trap wall. Since the trap asymmetry is large, it may be assumed to be the dominant cause of plasma expansion. Under these conditions, the plasma expansion rate is found[29] to scale as $B^{-0.65}$. A combination of asymmetric fields and electron–neutral collisions might lead to the scaling observed in the EDG device. As indicated earlier, at high enough pressure electron–neutral collisions are expected to be the dominant cause of plasma expansion, and the expansion rate is expected to scale as B^{-2}. While this is a planned subject for future experimental study on the EDG device, the present investigations are restricted to pressures where the electron temperature profile can be assumed to be approximately uniform[3,5] in the expanding plasma, and thus utilize the theoretical predictions given in Eqs. (4) and (5).

IV. DYNAMICS OF THE $m=1$ DIOCOTRON MODE

The $m=1$ diocotron mode[30–33] can be detected through the image charge induced in the trap walls. In the EDG device,[3–6] one of the colinear cylinders is divided axially into two half-cylinders. As the mode rotates azimuthally, the image charges also rotate azimuthally, causing an electron current to flow across the half-cylinders. In principal, any odd-numbered mode ($m=1,3,\ldots$) can be measured, but in the experiments described here, only the $m=1$ mode has been observed. The image currents are measured by adding an impedance between the sector probe and ground,[3] resulting in a measurable voltage. In the EDG device, the impedance is given by a capacitance of 1.3 nF in parallel with a resistance of 10 MΩ. The real part of this impedance, which leads to resistive wall destabilization, is between 0.05 Ω and 2 Ω for typical frequencies between 50 and 200 kHz.

A. Resistive-wall instability

One of the strongest factors affecting the stability of the $m=1$ diocotron mode in a Malmberg–Penning trap plasma with a monotonically-decreasing density profile is resistive-wall destabilization.[34] Physically, a resistive wall dissipates energy, and because the $m=1$ mode is a negative-energy mode, the mode amplitude and the displacement of the plasma column from the cylinder axis grow with the small-signal growth rate[34]

$$\gamma_R=\frac{1}{\pi^2}\frac{L_s^2}{L_p}\omega^2\sin^2\left(\frac{\Delta\theta}{2}\right)\left(\frac{R}{1+(\omega RC)^2}\right). \tag{8}$$

In the EDG device, the isolated sectors of the divided cylinder have axial length $L_s=5.08$ cm and azimuthal span $\Delta\theta=\pi$. In Fig. 8, the resistively destabilized $m=1$ diocotron mode amplitude D/R_w is plotted as a function of time. A resistance R of 3.1 kΩ is attached to the trap wall at the

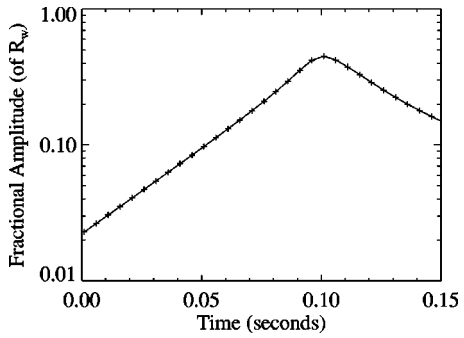

FIG. 8. The $m=1$ diocotron mode amplitude D/R_w is plotted versus time on a log-linear scale. The mode is destabilized with a 3.1 kΩ resistance, leading to an exponential increase in the mode amplitude. The mode saturates due to contact with the trap wall.

sector opposite to the sector probe, and the mode frequency is $\omega/2\pi=38.1$ kHz. The mode exhibits an exponential rate of growth (note the log-linear scale) until saturation occurs at 0.10 s. The saturation is believed to be due to plasma contact with the trap wall, and is accompanied by a decrease in the plasma line density. The initial amplitude of $D/R_w\simeq 0.02$ corresponds to a displacement of 0.05 cm, while the saturation amplitude corresponds to 1.25 cm.

The $m=1$ diocotron mode growth rates have been measured in the EDG device[3] over a wide range of resistances, and are shown in Fig. 9. The growth rates in Fig. 9 are measured while keeping a constant diocotron frequency $\omega/2\pi=38.0$ kHz, plasma length $L_p=15$ cm, and capacitance $C=200$ pF. The theoretical growth rate given in Eq. (8) is also plotted in Fig. 9. For low resistances with $\omega RC\ll 1$, the growth rate in Eq. (8) increases linearly with the resistance R. At $\omega RC=1$ there is a roll-over in the predicted growth rate, and for $\omega RC\gg 1$, the growth rate in Eq. (8) decreases as R^{-1}.

It is clear from Fig. 9 that measured growth rates are in excellent agreement with the theoretical predictions for all resistances between 17 Ω and 10^6 Ω, representing 2.5 orders-of-magnitude in growth rate. These measurements[3] not only reproduce previously published data,[34] but extend the data to both a *lower* and a *higher* range of resistances, and to smaller growth rates. The same level of agreement between the experimental data and theoretical predictions is found over the

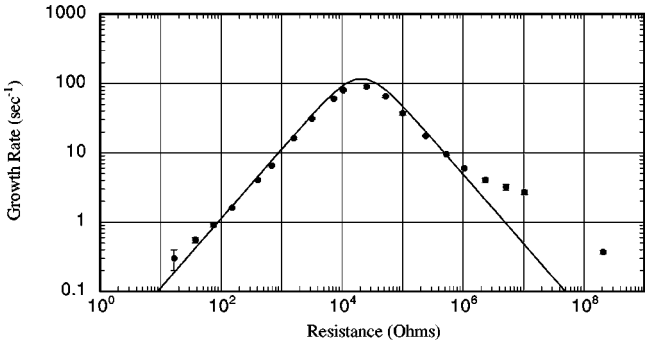

FIG. 9. The measured growth rates due to resistive wall destabilization are plotted versus resistance R, together with the absolute predictions of Eq. (8) for a wide range of wall resistances.

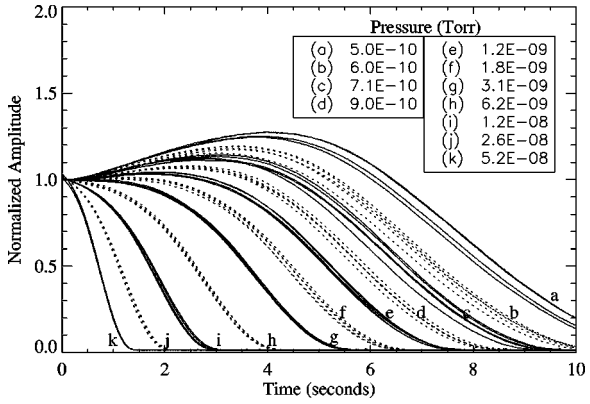

FIG. 10. The evolution of the amplitude of the $m=1$ diocotron mode is shown for eleven different background helium pressures, ranging from 5×10^{-10} Torr to 5×10^{-8} Torr. The solid and dotted curves are used to distinguish between pressures. At each pressure, five measurements of the mode evolution are shown.

range of 10^2 Ω to 10^6 Ω examined previously.[34] Outside this range, the measured growth rates are somewhat larger than the predictions, especially at resistances greater than 10^6 Ω. The cause of the discrepancy at large resistances is still under investigation.

B. Effects of background neutral pressure on the nonlinear evolution of the $m=1$ diocotron mode

We now consider the effects of collisions with background gas atoms on the dynamics of the $m=1$ diocotron mode. A recent calculation[35] predicts that elastic collisions between electrons and background neutrals can induce an instability in the (negative energy) $m=1$ diocotron mode, with characteristic small-signal growth rate $\gamma_n=\nu_{en}\omega_\infty/\omega_{ce}$. Here, ν_{en} is the electron–neutral collision frequency, $\omega_{ce}=eB/m_ec$ is the electron gyrofrequency, and $\omega_\infty=2ecN_L/R_w^2B$ is the $m=1$ diocotron frequency for an infinite-length plasma column. The calculation[35] assumes that the expansion of the plasma is sufficiently slow that the radial density profile can be regarded as stationary on the time scale of the instability. In the experiments on the EDG device, however, the expansion rate is observed to be faster than that expected due to electron–neutral collisions alone,[3–5] and also faster than the predicted characteristic exponentiation time[35] of the instability. Although providing initial motivation for the measurements of the diocotron mode, this theoretical model[35] is not expected to predict correctly the behavior of the diocotron mode in the EDG device.

The effects of electron–neutral collisions on the $m=1$ diocotron mode evolution are studied in the EDG device by injecting purified helium gas into the vacuum vessel while monitoring the evolution of the $m=1$ diocotron mode.[3] The amplitude evolution for eleven different background gas pressures is shown in Fig. 10 for a constant magnetic field strength of 612 G, and diocotron mode frequency of 55 kHz. The solid and dotted curves in Fig. 10 are used to distinguish between pressures, and at each pressure five measurements of the mode evolution are shown. The amplitudes plotted in Fig. 10 are normalized to the initial amplitude for clarity,

even though the initial amplitudes are approximately equal (to within 10%). The mode frequencies are constant as a function of time (to within 1%) even as the mode amplitude decays to zero, indicating that no charge is lost during the measured evolution.

From Fig. 10, a nonexponential damping of the $m=1$ diocotron mode is observed, which becomes stronger as the background neutral pressure is increased. The solid curves labeled ''a'' show the amplitude evolution at the base pressure of 5×10^{-10} Torr. A slight increase in the mode amplitude is evident initially, possibly due to small wall resistance, with an equivalent exponential growth rate of less than $0.1\,s^{-1}$. The ''dotted'' curves labeled ''b'' show the amplitude evolution after helium has been injected to increase the measured pressure to 6×10^{-10} Torr (N_2 equivalent), a difference of only 1×10^{-10} Torr from the base pressure. At this pressure, the diocotron mode evolution is measurably different, with good reproducibility, and with the amplitude decaying to nearly zero by 10 s. As the background gas pressure is increased further, the diocotron mode damping rate becomes greater.

The sensitivity of the diocotron mode evolution to changes in the background gas pressure of as little as 1×10^{-10} Torr is somewhat surprising in view of the expansion data in Sec. III, where it appears that for pressures lower than 1×10^{-8} Torr the plasma expansion rate is independent of pressure. However, the data in Fig. 6 required many hundreds of repeated plasma shots to obtain each data point, and variations in the experimental parameters over the long times necessary to obtain the data obscure the expansion rate dependence on the background gas pressure at very low pressures. By contrast, the evolution of the diocotron mode presented in Fig. 10 can be measured in a single plasma shot, and therefore, small changes in the background gas pressure can be more readily measured while keeping other experimental parameters constant.

To conveniently characterize the nonexponential damping shown in Fig. 10, the time τ for the mode amplitude to decay to one-half of its initial amplitude is plotted as a function of the background gas pressure P in Fig. 11. Also shown is the time for the amplitude to decay to one-tenth of its initial amplitude. A power law fit is performed on both sets of data which indicates that the time τ is approximately proportional to $P^{-1/2}$. A consistent explanation of the nonexponential rate of damping and the $P^{-1/2}$ scaling of τ are still being sought. The nonexponential rate of damping could be explained if the damping were due to plasma proximity with the trap walls. The amplitude evolution would then be expected to look similar to those in Fig. 10, with very little decay initially because the plasma is far from the trap walls, and more rapid decay later in time as the plasma expansion brings the plasma closer to the trap walls. However, since the plasma is expected to expand at a rate proportional to the background gas pressure P, the time for the mode to damp would be expected to be proportional to P^{-1}. To investigate the cause of the mode damping further, more experiments are needed which measure the density profile evolution during the mode damping. In any case, from Figs. 10 and 11, the strong sensitivity of the evolution of the $m=1$ diocotron mode to the background neutral gas pressure has been clearly demonstrated in the EDG device.

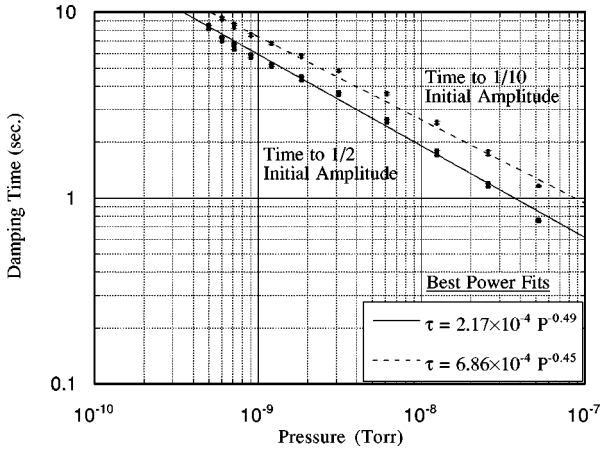

FIG. 11. The time τ for the measured $m=1$ diocotron mode amplitude to decay to one-half of the initial amplitude is plotted as a function of the background gas pressure. Also plotted is the time for the mode to decay to one-tenth of the initial amplitude. The vertical width of the bars are the maximum and minimum times for this to occur, as determined from the data shown in Fig. 9.

V. CONCLUSIONS

In this paper, we have discussed the effects of background neutral gas on the dynamics of a pure electron plasma confined in the Electron Diffusion Gauge (EDG) device. Following a description of the experimental setup in Sec. II, detailed experimental results were presented in Sec. III, which describe how the plasma expansion rate scales with background helium gas pressure P (Fig. 6) and magnetic field strength B (Fig. 7) based on direct measurements of the expanding density profile $n(r,t)$. While the expansion rate is sensitive to background gas pressure at pressures exceeding 10^{-8} Torr (Fig. 6), at lower pressures the cross-field transport observed in repeated hold-and-dump measurements of the expanding density profile appears to be dominated by other processes, e.g., asymmetry-induced transport. Finally, in Sec. IV, using single-shot measurements, it was shown that the nonlinear evolution of the $m=1$ diocotron mode exhibits a very sensitive dependence on the background helium gas pressure P (Fig. 10), and that the characteristic time scale τ for damping of the diocotron mode scales as $P^{-1/2}$ (Fig. 11) for background helium pressures ranging from 5×10^{-10} Torr to 5×10^{-8} Torr. Sensitivities to pressure variations as small as 10^{-10} Torr are observed (Fig. 11). Given the strong sensitivity of the diocotron mode measurements to background gas pressure, future research will focus (for example) on determining properties of the diocotron mode evolution at pressures below 5×10^{-10} Torr; determining the effects of changing the ratio of initial plasma radius to wall radius (R_{p0}/R_w) on the diocotron mode evolution; installation of a temperature diagnostic to determine the degree to which the electron temperature remains uniform during the plasma evolution; and development of a theoretical model that describes (qualitatively at least) the $P^{-1/2}$ scaling of the characteristic damping time τ of the diocotron mode.

ACKNOWLEDGMENT

This research was supported by the Office of Naval Research.

[1]R. C. Davidson, *Physics of Nonneutral Plasmas* (Addison-Wesley, Reading, MA, 1990), and references therein.
[2]T. M. O'Nell, Phys. Today **52**, 24 (1999).
[3]E. H. Chao, Ph.D. thesis, Princeton University (1999).
[4]E. H. Chao, R. C. Davidson, S. F. Paul, and K. A. Morrison, Proceedings of the 1999 Workshop on Nonneutral Plasmas (Princeton University, 1999); American Institute of Physics Conference Proceedings, No. 498, edited by J. Bollinger, R. C. Davidson, and R. Spencer (American Institute of Physics, Melville, NY, 1999), p. 278.
[5]E. H. Chao, R. C. Davidson, and S. F. Paul, J. Vac. Sci. Technol. A **17**, 2050 (1999), and references therein.
[6]E. H. Chao, S. F. Paul, and R. C. Davidson, J. Vac. Sci. Technol. A **17**, 2034 (1999), and references therein.
[7]R. C. Davidson and D. A. Moore, Phys. Plasmas **3**, 218 (1996).
[8]R. C. Davidson and E. H. Chao, Phys. Plasmas **3**, 2615 (1996).
[9]J. J. Bollinger, J. D. Presage, W. M. Itano, and D. J. Wineland, Phys. Rev. Lett. **54**, 1000 (1985).
[10]J. J. Bollinger and D. J. Wineland, Phys. Plasmas **1**, 1403 (1994).
[11]C. F. Driscoll and K. S. Fine, Phys. Fluids B **2**, 1359 (1990).
[12]C. F. Driscoll, in *Research Trends in Physics: Nonlinear and Relativistic Effects in Plasmas*, edited by V. Stefan (American Institute of Physics, New York, 1992), p. 454.
[13]X. P. Huang and C. F. Driscoll, Phys. Rev. Lett. **72**, 2187 (1994).
[14]F. Anderegg, X. P. Huang, C. F. Driscoll, E. M. Hollmann, T. M. O'Neil, and D. H. E. Dubin, Phys. Rev. Lett. **78**, 2128 (1997).
[15]T. M. O'Neil and D. H. F. Dubin, Phys. Plasmas **5**, 2163 (1998).
[16]D. H. E. Dubin and T. M. O'Neil, Rev. Mod. Phys. **71**, 20 (1999).
[17]C. M. Surko, M. Leventhal, and A. Passner, Phys. Rev. Lett. **62**, 901 (1989).
[18]C. M. Surko and T. J. Murphy, Phys. Rev. B **2**, 1372 (1990).
[19]R. G. Greaves, M. D. Tinkle, and C. M. Surko, Phys. Plasmas **1**, 1439 (1994).
[20]A. R. Filippelli and S. Dittmann, J. Vac. Sci. Technol. A **9**, 2757 (1991).
[21]P. C. Arnold and S. C. Borichevsky, J. Vac. Sci. Technol. A **12**, 568 (1994).
[22]J. H. Malmberg and J. S. deGrassie, Phys. Rev. Lett. **35**, 577 (1975).
[23]J. M. Kriesel and C. F. Driscoll, Phys. Plasmas **5**, 1265 (1998).
[24]E. H. Chao, R. C. Davidson, S. F. Paul, and K. S. Fine, Proceedings of the 1999 Workshop on Nonneutral Plasmas (Princeton University, 1999); American Institute of Physics Conference Proceedings, No. 498, edited by J. Bollinger, R. C. Davidson, and R. Spencer (American Institute of Physics, Melville, New York, 1999), p. 461.
[25]D. L. Eggleston, C. F. Driscoll, B. R. Beck, A. W. Hyatt, and T. H. Malmberg, Phys. Fluids B **4**, 3432 (1992).
[26]See, for example, Fig. 2 of Ref. 5.
[27]J. H. Malmberg and C. F. Driscoll, Phys. Rev. Lett. **44**, 654 (1980).
[28]J. S. deGrassie and J. H. Malmberg, Phys. Fluids **23**, 63 (1980).
[29]J. Notte and J. Fajans, Phys. Plasmas **1**, 1123 (1994).
[30]R. Levy, Phys. Fluids **11**, 920 (1968).
[31]K. S. Fine, Ph.D. thesis, University of California, San Diego (1988).
[32]C. F. Driscoll and K. S. Fine, Phys. Fluids B **23**, 1359 (1990).
[33]K. S. Fine and C. F. Driscoll, Phys. Plasmas **5**, 601 (1998).
[34]W. D. White, J. H. Malmberg, and C. F. Driscoll, Phys. Rev. Lett. **49**, 1822 (1982).
[35]R. C. Davidson and E. H. Chao, Phys. Plasmas **3**, 3279 (1996).